Supporting Information

Molecularly Tailored Perovskite/Poly(3-hexylthiophene) Interfaces for High-performance Solar Cells

Ming-Hua Li,‡ [ab] Xinbo Ma,‡[c] Jiaju Fu,[a] Shuo Wang,[a] Jinpeng Wu,[a] Run Long,*[c] and Jin-Song Hu*[ad]

[a] Beijing National Laboratory for Molecular Sciences (BNLMS), Institute of Chemistry, Chinese Academy of Sciences, Beijing 100190, China

[b] College of Chemical Engineering, Beijing Advanced Innovation Center for Soft Matter Science and Engineering, Beijing University of Chemical Technology, Beijing 100029, China

[c] Key Laboratory of Theoretical & Computational Photochemistry of Ministry of Education, College of Chemistry, Beijing Normal University, Beijing 100875, China

[d] School of Chemical Sciences, University of Chinese Academy of Sciences, Beijing 100049, China

‡ These authors contributed equally to this work.

* Corresponding author. E-mail: runlong@bnu.edu.cn (R. L.); hujs@iccas.ac.cn (J. H.)

Materials and Methods

Materials

The raw materials of Cesium iodide (CsI, 99.999%), lead iodide (PbI_2, 99.999%), lead bromide ($PbBr_2$, 99.999%), dimethylformamide (DMF, anhydrous, ≥99.9%), dimethyl sulfoxide (DMSO, anhydrous, ≥99.9%), chlorobenzene (anhydrous, 99.8%) were purchased from Sigma-Aldrich. Dimethylammonium iodide (DMAI) was purchased from Greatcell Solar. Tris[2-(diphenylphosphino)ethyl]phosphine (PP3, 98%) and other phosphorus-based molecules were purchased from Strem. Poly(3-hexylthiophene) (P3HT) was purchased from 1-Material. Tin (IV) oxide (SnO_2) colloidal solution (15% in H_2O) was purchased from Alfa Aesar. Titanium (IV) chloride ($TiCl_4$) was purchased from Aladdin. The patterned ITO and FTO glass substrates were purchased from Advanced Election Technology.

Precursor Preparation

The precursor of SnO_2 compact layer was prepared by dissolving SnO_2 colloidal solution with DI water by a weight ratio of 1 : 5. 1.2 mmol CsI, 0.6 mmol PbI_2, and 0.6 mmol $PbBr_2$ were mixed in 1 mL DMSO to form the $CsPbI_2Br$ precursor. 1 mmol CsI, 1 mmol PbI_2, and 1 mmol DMAI were mixed in 0.9 mL DMF and 0.1 mL DMSO to form the $CsPbI_3$ precursor. 1.8 mmol PbI_2, 1.8 mmol FAI, 0.036 mmol CsCl and 0.63 mmol MACl were mixed in 0.8 mL DMF and 0.2 mL DMSO to form the $CsFAPbI_3$ precursor. The different concentrations of PP3 or other phosphine molecules were dissolved in chlorobenzene. The P3HT hole transporting layer solution was prepared by dissolving 10 mg P3HT in 1 mL chlorobenzene.

Device Fabrication

The SnO_2 precursor was spin-coated at 4000 rpm for 30 s on the pre-cleaned ITO substrates and followed by annealing at 150 ^oC for 30 min in ambient conditions. The inorganic perovskite films were deposited according to our optimized preannealing method. The $CsPbI_2Br$ precursor was spin-coated at 2000 rpm for 120 s and followed by annealing at 50 ^oC for 2 min and 160 ^oC for 10 min. It must be noted that carefully controlling the preannealing process is very critical for achieving highly crystalline perovskite films. Then, the PP3 solution was spin-coated on the inorganic perovskite film at 5000 rpm for 30 s and annealed at 100 ^oC for 5 min to evaporate the solvent. The P3HT solution was dynamically spin-coated at 3000 rpm for 30 s and annealed at 100

°C for 5 min to improve the interface contact. Finally, Au layers (about 80 nm) were thermally evaporated to complete the device.

For the $CsPbI_3$ PSCs, the $CsPbI_3$ precursor was spin-coated on the pre-heated FTO/TiO_2 substrates at 3000 rpm for 30 s and followed by annealing at 190 °C for 12 min in air. The PP3 solution (5 mM) was subsequently spin-coated on the perovskite film and followed by annealing at 100 °C for 5 min. The other procedures are consistent with the $CsPbI_2Br$ PSCs.

For the $CsFAPbI_3$ PSCs, the $CsFAPbI_3$ precursor was spin-coated on FTO/SnO_2 substrate at 5000 rpm for 30 s and 1 mL was dropped on the spinning substrate 10 s before the end. The as-cast films were annealed at 70 °C for 5 min and 120 °C for 30 min. Precise humidity control is important for high-quality perovskite films and device performance. The PP3 solution (5 mM) was subsequently spin-coated on the perovskite film and followed by annealing at 100 °C for 5 min. The other procedures are consistent with the $CsPbI_2Br$ PSCs.

Film and Device Characterization

The absorption spectra were carried out by UV/vis spectrophotometer (Hitachi, UH-4150). The SEM images were captured by Field-Emission Scanning Electron Microscope (Hitachi, SU4800). The XRD diffraction patterns were conducted by Rigaku DMAX-RB with a Cu-Kα X-ray radiation source. Steady-state and time-resolved photoluminescence spectra were measured by Edinburgh Instruments (FLS980). The impedance spectroscopy was carried out by an electrochemical workstation (CHI 660E). The EQE spectra were measured by QE-R3011 (Enlitech) system. The X-ray photoelectron spectroscopy (XPS) and ultraviolet photoelectron spectroscopy (UPS) were detected by a combined XPS/UPS system (Thermo Fisher Scientific, ESCALAB250XI). The *J-V* curves were measured by an ORIEL measurement system with Keithley 2420 source under simulated AM 1.5G irradiation (Oriel Sol3A Class AAA solar simulator, 450W Model 94023A, Newport). The irradiation was calibrated by a certified silicon reference cell (91150-KG5, Newport). The devices were measured under reverse scan (1.2 to -0.2 V) or forward scan (-0.2 to 1.2 V) with a rate of 0.02 V s^{-1} in ambient conditions below 30% RH. There were no special preconditioning protocols applied before device measurement. The active area was defined by an opaque aperture with a certified area of 0.0895 cm^2. For the storage stability test, unencapsulated devices were stored in an air atmosphere with ≤30% RH at 25 ± 5 °C. For the thermal stability test, unencapsulated devices were continuously heated on a hotplate at 85 °C in

N_2. For long-term operational stability, the encapsulated devices were continuously illuminated in air.

Computational Details

The projector-augmented wave (PAW) method using Vienna Ab initio Simulation Package (VASP) was utilized to carry out DFT calculations. The crystal structure of cubic $CsPbI_2Br$ bulk structure and slabs were optimized by a generalized gradient approximation (GGA) with Perdew–Burke–Ernzerhof (PBE) method. The structural optimization (self-consistent) was defined by plane-wave cutoff energy at 400 eV and a 1 × 1 × 1 Γ point. The structural optimizations and electronic calculations were also carried out by the van der Waals functional vdW-DF3. Surface slabs with a vacuum thickness of 18 Å were modeled as (001)-terminated slabs of the cubic structure. Two-layer supercell of the 4 × 4 surface was used. All the structures were optimized until the force on each atom was smaller than 0.02 eV $Å^{-1}$ and the convergence threshold for self-consistent iteration is 10^{-5} eV. The molecular graphics viewer VESTA was used to plot the crystal structures and charge densities.

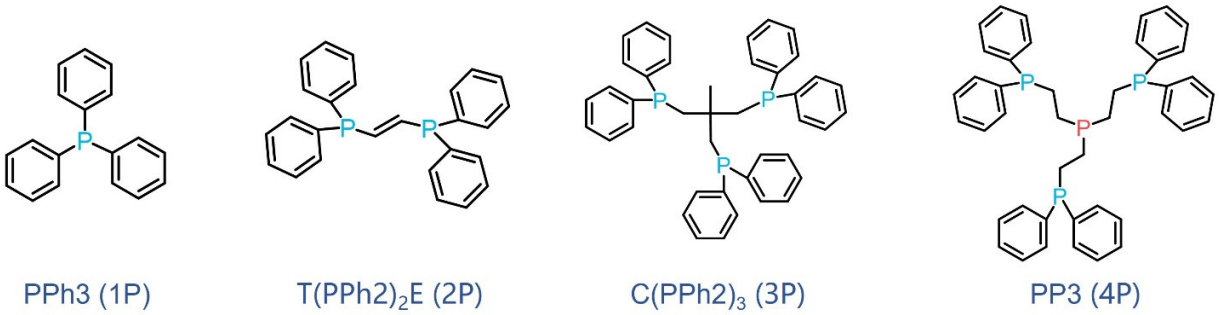

Fig. S1. Chemical structure of phosphine ligands.

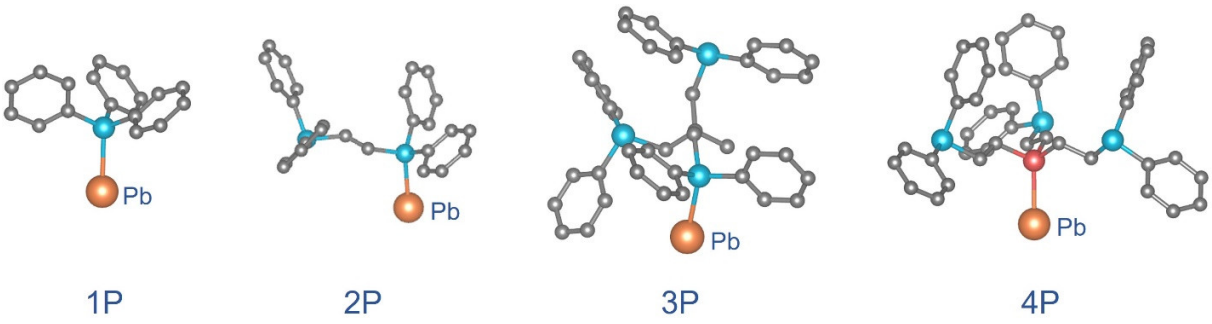

Fig. S2. Simulated interaction model between phosphine ligands and Pb.

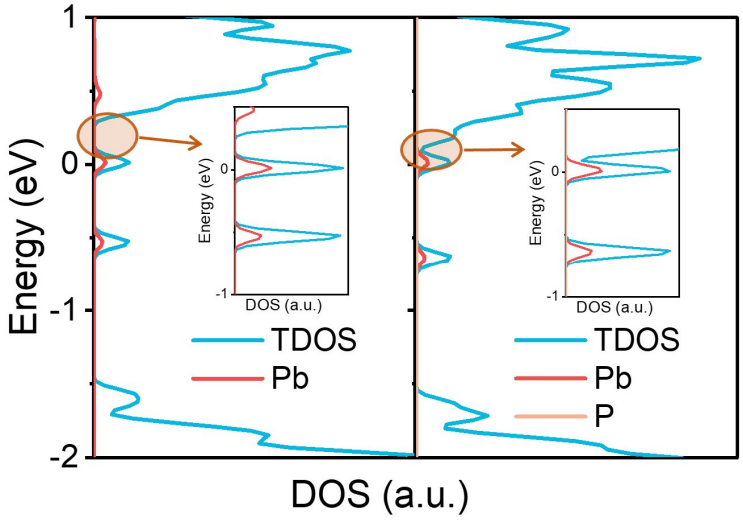

Fig. S3. Density of state of $CsPbI_2Br$ with and without PP3 treatment.

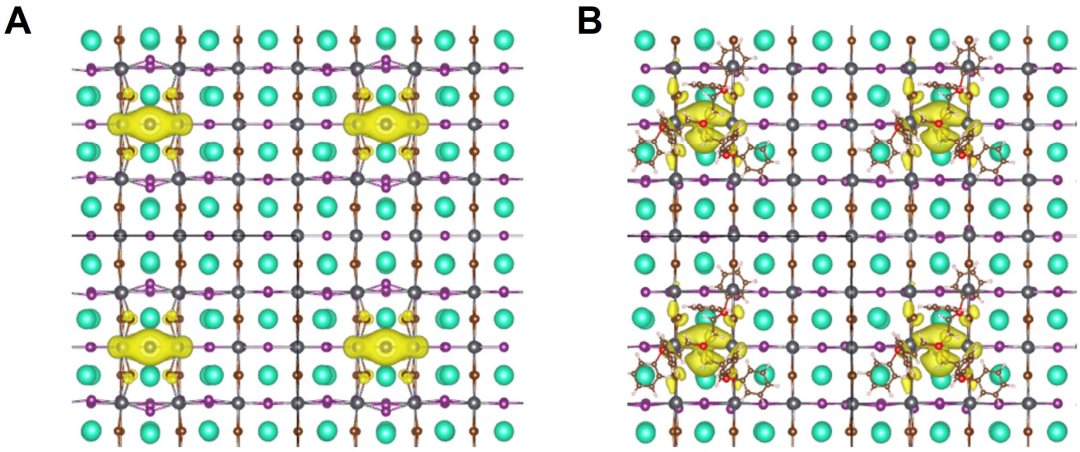

Fig. S4. Charge densities of defect state with higher energy level in (A) $CsPbI_2Br$ with antisite defect and (B) $CsPbI_2Br$ with antisite defect under PP3 treatment.

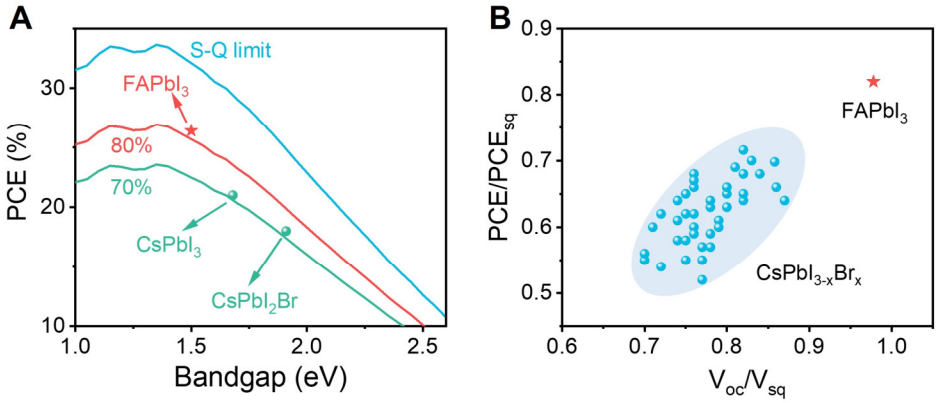

Fig. S5. Photovoltaic parameters analysis of reported high-efficiency PSCs.

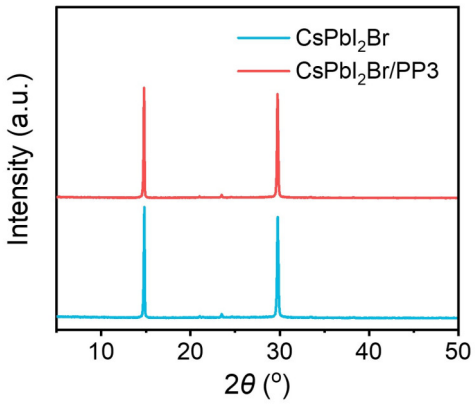

Fig. S6. XRD patterns of $CsPbI_2Br$ with and without PP3 treatment.

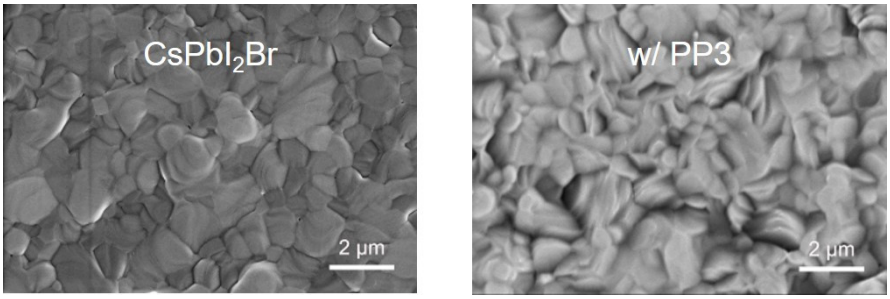

Fig. S7. Top-view SEM images of $CsPbI_2Br$ and $CsPbI_2Br$/PP3 films.

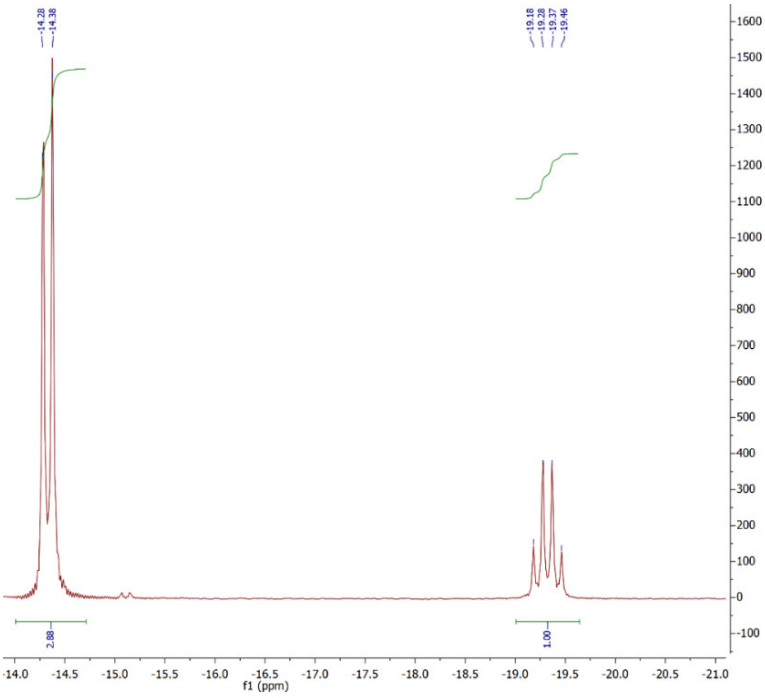

Fig. S8. The ^{31}P NMR spectrum of PP3.

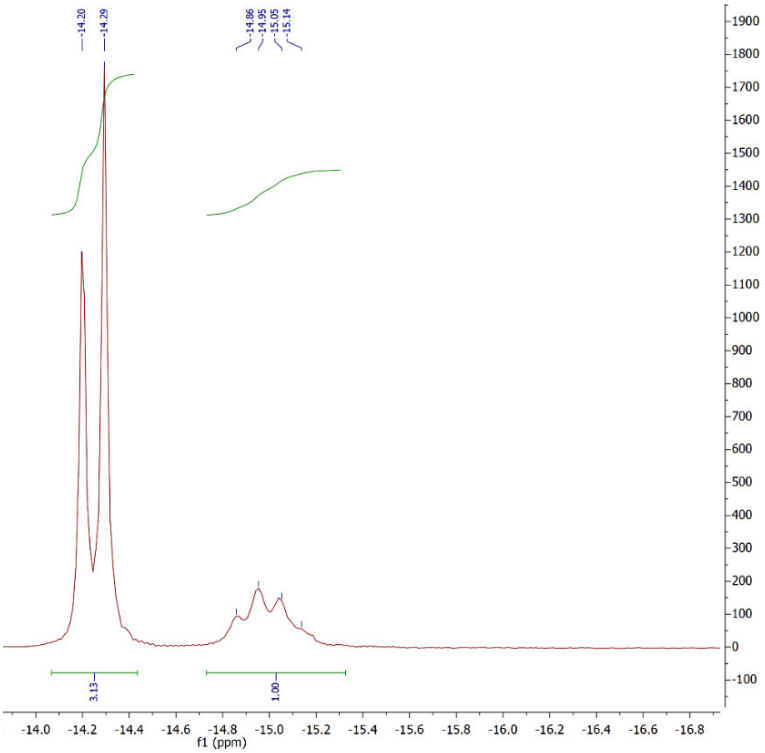

Fig. S9. The ^{31}P NMR spectrum of $CsPbI_2Br$/PP3.

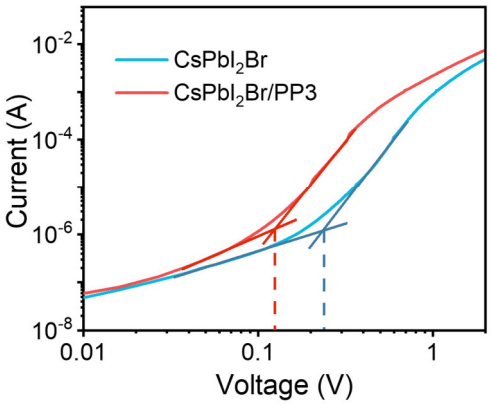

Fig. S10. SCLC measurements.

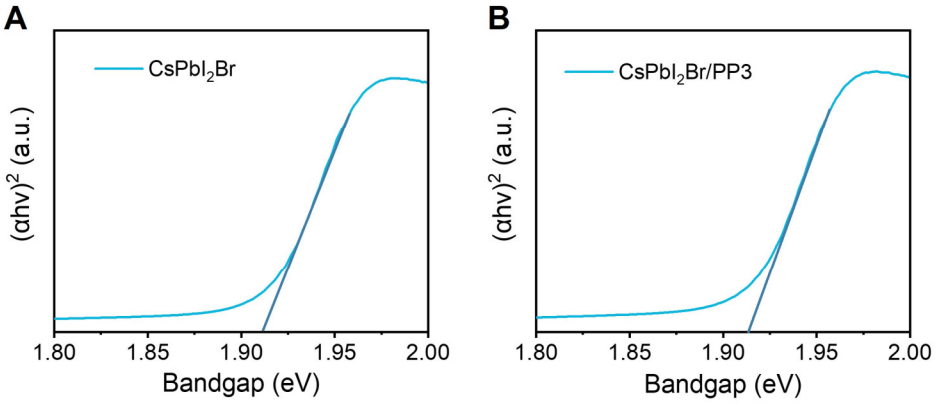

Fig. S11. Tauc plots of (A) $CsPbI_2Br$ and (B) $CsPbI_2Br$/PP3 films.

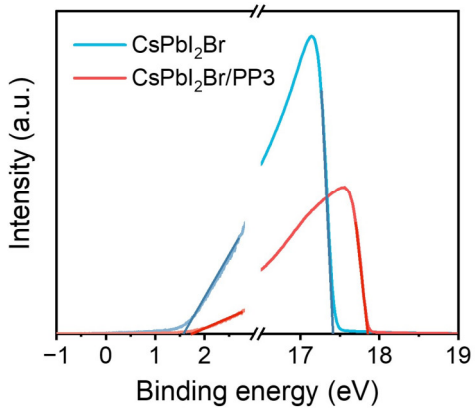

Fig. S12. UPS spectra.

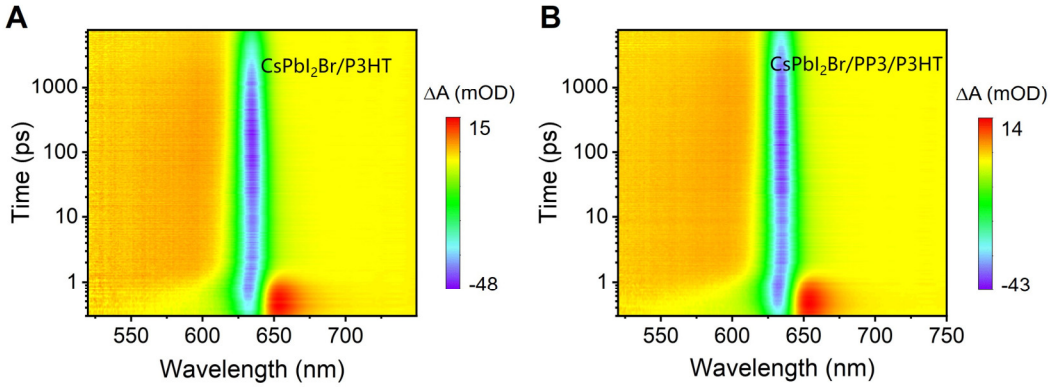

Fig. S13. 2D TA images of (A) $CsPbI_2Br$/P3HT and (B) $CsPbI_2Br$/PP3/P3HT samples.

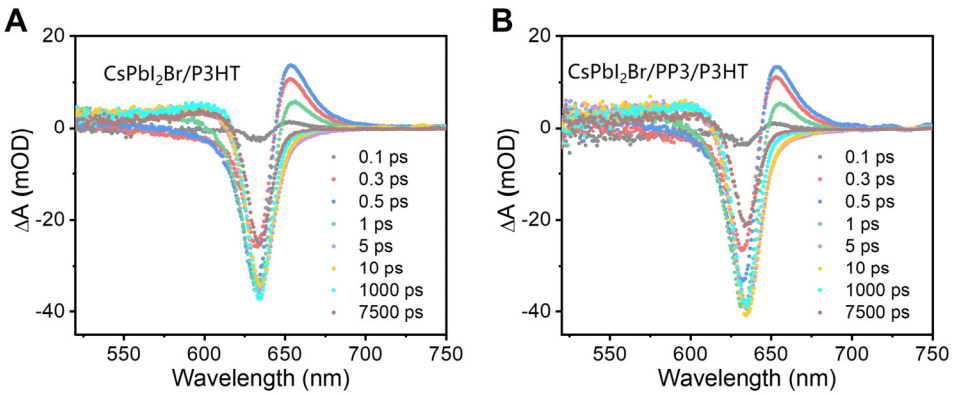

Fig. S14. TA spectra of $CsPbI_2Br$/P3HT samples (A) without and (B) with PP3 treatment under different probe times.

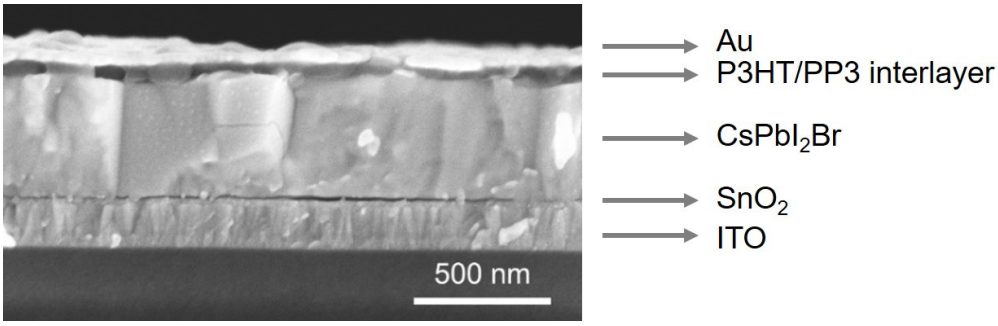

Fig. S15. Cross-sectional SEM image of the best PSC with an architecture of ITO/SnO_2/$CsPbI_2Br$/PP3/dopant-free P3HT/Au.

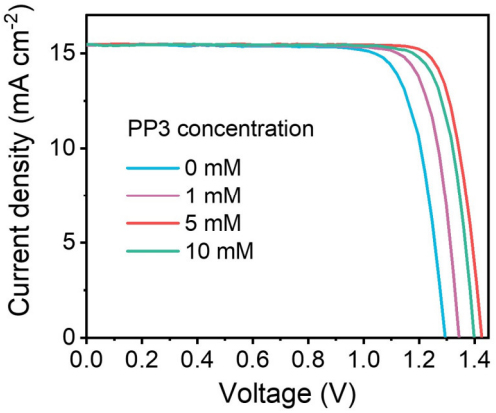

Fig. S16. J-V curves of $CsPbI_2Br$ PSCs with different PP3 concentrations.

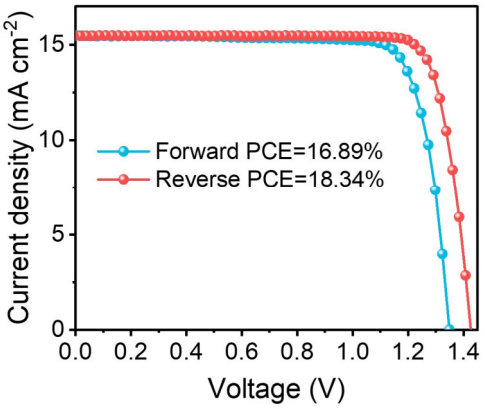

Fig. S17. J-V curves of the $CsPbI_2Br$ PSC measured at different scan directions.

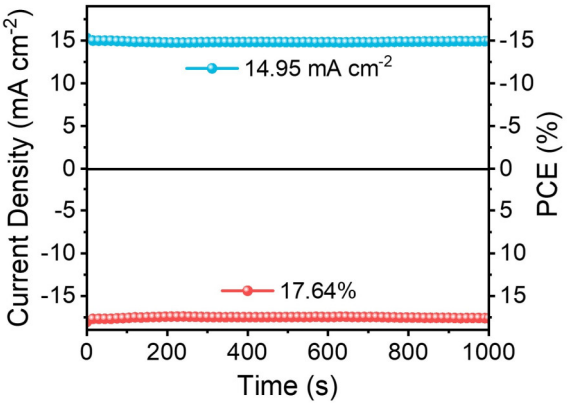

Fig. S18. Time-dependent stabilized power output of the $CsPbI_2Br$ PSC.

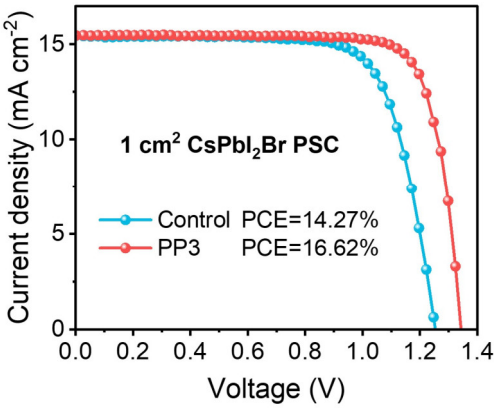

Fig. S19. J-V curves of 1 cm^2 $CsPbI_2Br$ PSCs with and without PP3 treatment.

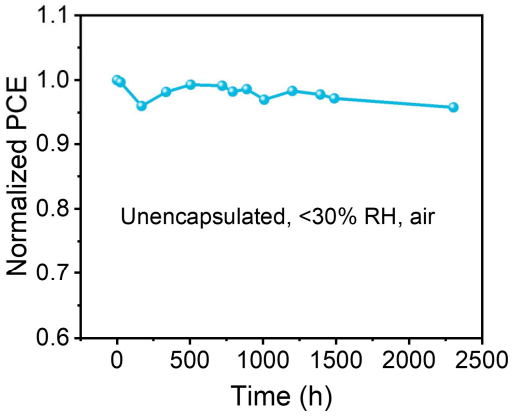

Fig. S20. Humidity stability test of unencapsulated $CsPbI_2Br$ PSC stored in air.

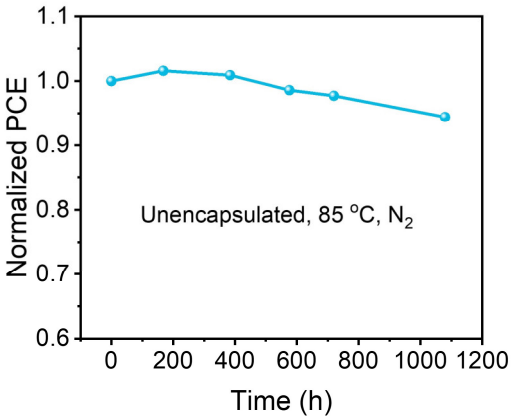

Fig. S21. Thermal stability test of unencapsulated $CsPbI_2Br$ PSC at 85 °C in N_2.

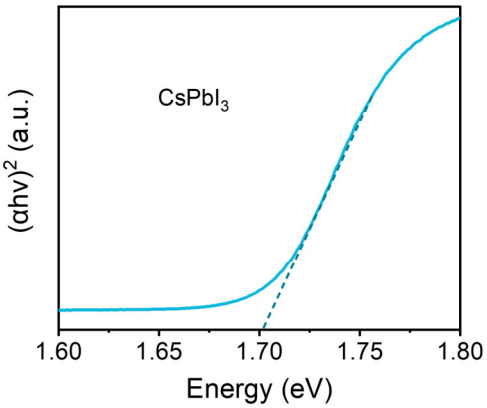

Fig. S22. Tauc plot of $CsPbI_3$ perovskite.

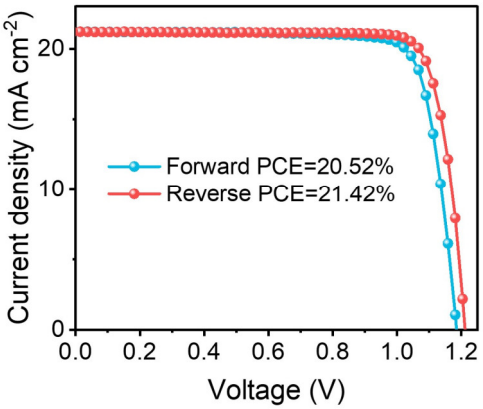

Fig. S23. J-V curves of $CsPbI_3$ PSCs measured under different scan directions.

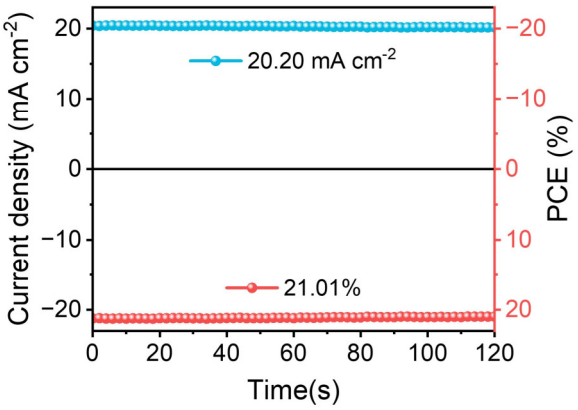

Fig. S24. Time-dependent stabilized power output of the $CsPbI_3$ PSC.

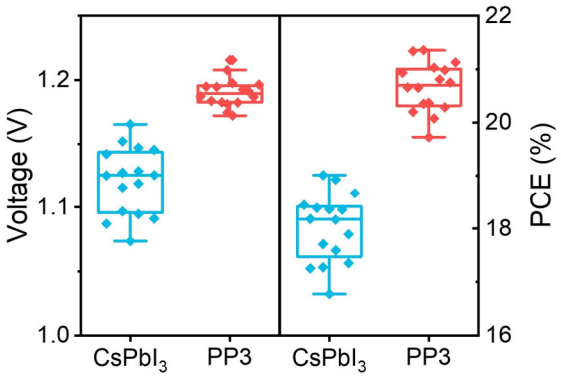

Fig. S25. Statistic V_{oc} and PCE distributions of $CsPbI_3$ PSCs.

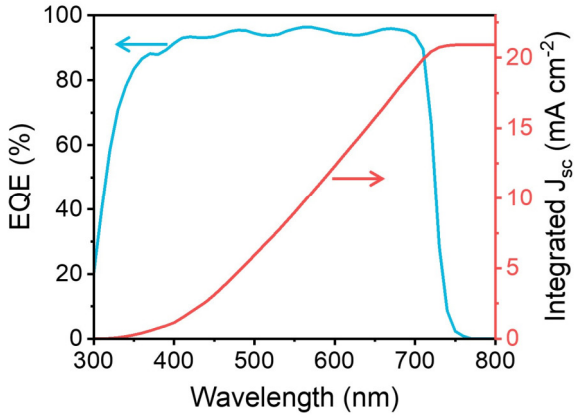

Fig. S26. EQE spectrum of the best $CsPbI_3$ PSC.

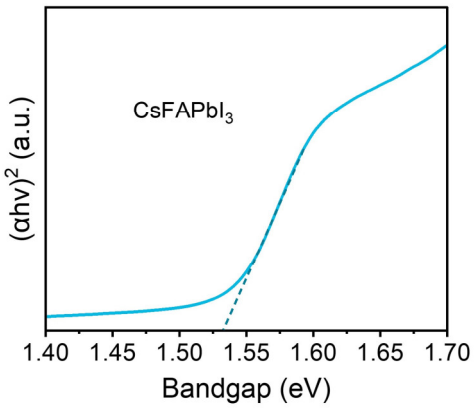

Fig. S27. Tauc plot of $CsFAPbI_3$ perovskite.

PHOTOVOLTAIC AND WIND POWER SYSTEMS QUALITY TEST CENTER, IEE, CHINESE ACADEMY OF SCIENCES

Report No: PWQC-WT-P23042021-1R

Sample code	DC2023a042
Sample S/N	3
Type	Single Junction Perovskite Solar Cell
Designated area	0.08955cm² The designated area was provided by National Institute of Metrology, China. Test Report No. CDjc2022-04430.

Items of testing	Measurement of photovoltaic current-voltage characteristics					
Sample code	DC2023a042					
Results	**Voltage Sweep**	**Isc** (mA)	**Jsc** (mA/ cm²)	**Voc** (V)	**Pm** (mW)	**File**
	Forward	2.320	25.908	1.159	2.182	A202304200 95623-f
		Ipm (mA)	**Vpm** (V)	**FF** (%)	**Eff** (%)	
		2.182	1.000	81.16	24.37	
	Voltage Sweep	**Isc** (mA)	**Jsc** (mA/ cm²)	**Voc** (V)	**Pm** (mW)	**File**
	Reverse	2.317	25.873	1.161	2.197	A202304200 95623-r
		Ipm (mA)	**Vpm** (V)	**FF** (%)	**Eff** (%)	
		2.154	1.020	81.71	24.54	

Measurement uncertainty:

$U_{95(Isc)}$=1.9% (k=2)

$U_{95(Voc)}$=1.8% (k=2)

$U_{95(Pm)}$=2.5% (k=2)

PHOTOVOLTAIC AND WIND POWER SYSTEMS QUALITY TEST CENTER, IEE, CHINESE ACADEMY OF SCIENCES

Report No: PWQC-WT-P23042021-1R

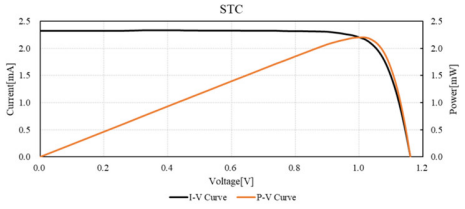

Type Single Junction Perovskite Solar Cell
Ser.No DC2023a042
Area 8.955 mm²
Isc 2.320 mA
Jsc 25.908 mA/cm²
Voc 1.159 V
FF 81.16 %
Pm 2.182 mW
Eff 24.37 %
Ipm 2.182 mA
Vpm 1.000 V
Voltage Sweep Forward
Sweep time 6.6 s
Temp 25 ℃
Irr 100 mW/cm²
File A20230420095623-f

PHOTOVOLTAIC AND WIND POWER SYSTEMS QUALITY TEST CENTER, IEE, CHINESE ACADEMY OF SCIENCES

Report No: PWQC-WT-P23042021-1R

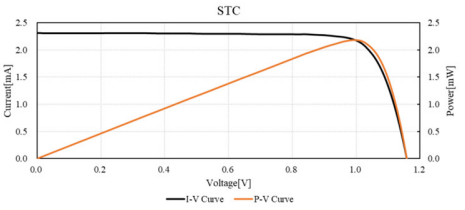

Type Single Junction Perovskite Solar Cell
Ser.No DC2023a042
Area 8.955 mm²
Isc 2.317 mA
Jsc 25.873 mA/cm²
Voc 1.161 V
FF 81.71 %
Pm 2.197 mW
Eff 24.54 %
Ipm 2.154 mA
Vpm 1.020 V
Voltage Sweep Reverse
Sweep time 6.6 s
Temp 25 ℃
Irr 100 mW/cm²
File A20230420095623-r

Fig. S28. Third-party certification report of the champion $CsFAPbI_3$/P3HT PSC.

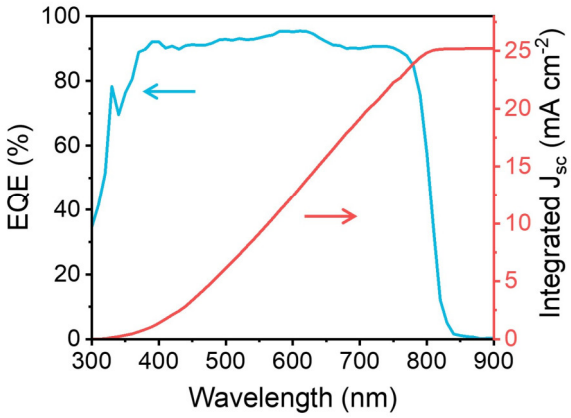

Fig. S29. EQE spectrum of the best $CsFAPbI_3$ PSC.

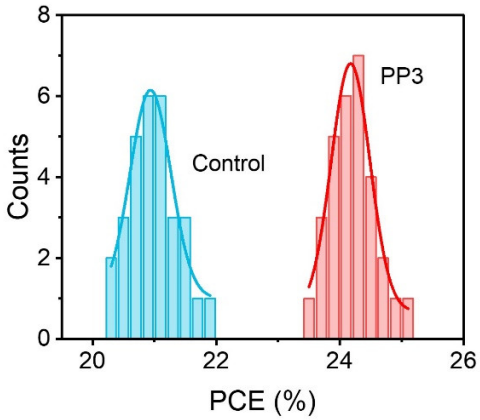

Fig. S30. Statistic PCE distributions of $CsFAPbI_3$ PSCs.

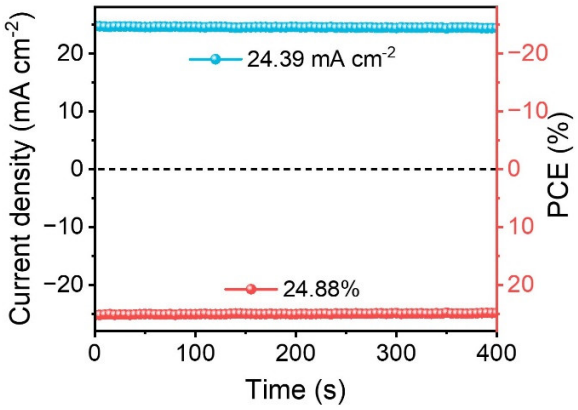

Fig. S31. Stabilized power output of the best $CsFAPbI_3$ PSC.

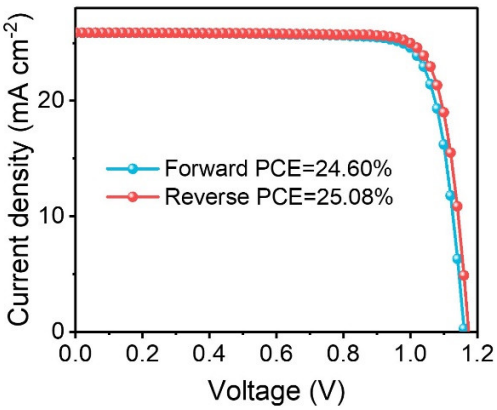

Fig. S32. J-V curves of the $CsFAPbI_3$ PSC measured at different scan directions.

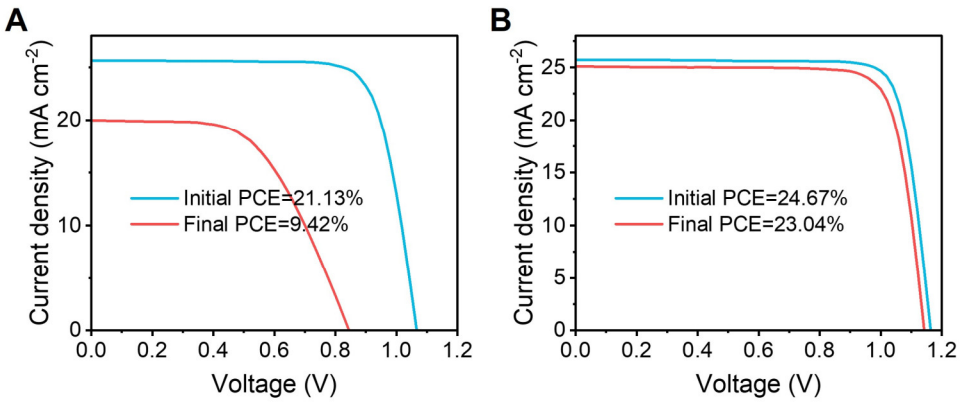

Fig. S33. J-V curves of the (A) control and (B) PP3-treated $CsFAPbI_3$ PSCs before and after operational stability test.

Table S1. Fitted results of time-resolved PL decay curves.

Condition	τ_1 (ns)	τ_2 (ns)	A_1 (%)	A_2 (%)	$\tau_{\text{-average}}$ (ns)
$CsPbI_2Br$	12.42	37.29	62.61	37.39	21.72
$CsPbI_2Br$/PP3	15.38	72.15	22.98	77.02	59.10

The results were fitted according to the bi-exponential function: $PL_{intensity} = A_1\exp(-t/\tau_1) + A_2\exp(-t/\tau_2)$. All the samples were directly deposited on glass substrates without a charge transfer layer.

Table S2. Summary of energy level parameters for control and PP3-treated $CsPbI_2Br$.

Condition	$E_{Cut\text{-}off}$ (eV)	WF (eV)	E_{Onset} (eV)	E_{VBM} (eV)	E_{CBM} (eV)	E_g (eV)
$CsPbI_2Br$	17.41	3.81	1.56	5.37	3.46	1.91
$CsPbI_2Br$/PP3	17.85	3.37	1.72	5.09	3.18	1.91

Table S3. Statistical photovoltaic parameters of control and PP3-treated $CsPbI_2Br$ PSCs.

Condition	V_{oc} (V)	J_{sc} (mA cm^{-2})	FF	PCE (%)
$CsPbI_2Br$	1.27±0.03	15.45±0.15	0.77±0.02	15.09±0.36
$CsPbI_2Br$/PP3	1.39±0.02	15.47±0.05	0.81±0.01	17.67±0.32

Table S4. Photovoltaic performance of $CsPbI_2Br$ PSCs with different concentrations of PP3 treatment.

Condition (mM/mL)	V_{oc} (V)	J_{sc} (mA cm^{-2})	FF	PCE (%)
0	1.29	15.43	0.792	15.79
1	1.34	15.44	0.819	16.96
5	1.43	15.46	0.832	18.39
10	1.40	15.46	0.819	17.72

Table S5. Summary of photovoltaic parameters for state-of-the-art inorganic $CsPbI_2Br$ PSCs with dopant-free HTLs.

HTL	Dopant	Perovskite	V_{oc} (V)	V_{oc} loss (V)	PCE (%)	Ref.
PSQ2	Free	$CsPbI_2Br$	1.27	0.64	15.50	[1]
TEP-S	Free	$CsPbI_2Br$	1.26	0.65	15.60	[2]
PBDB-T-Si	Free	$CsPbI_2Br$	1.20	0.71	15.60	[3]
PDCBT	Free	$CsPbI_2Br$	1.24	0.67	16.41	[4]
PBDB-T	Free	$CsPbI_2Br$	1.24	0.67	16.40	[5]
PolyTPD	Free	$CsPbI_2Br$	1.24	0.67	16.84	[6]
SFDT-TDM	Free	$CsPbI_xBr_{3-x}$	1.28	0.54	17.10	[7]
NiOx	Free	$CsPbI_2Br$	1.30	0.61	17.02	[8]
P3HT	Free	$CsPbI_xBr_{3-x}$	1.12	0.63	14.08	[9]
P3HT	Free	$CsPbI_xBr_{3-x}$	1.12	0.63	15.84	[10]
P3HT	Free	$CsPbI_2Br$	1.27	0.64	10.8	[11]
P3HT	Free	$CsPbI_2Br$	1.07	0.84	11.30	[12]
P3HT	Free	$CsPbI_2Br$	1.15	0.76	12.46	[13]
P3HT	Free	$CsPbI_2Br$	1.23	0.69	13.25	[14]
P3HT	Free	$CsPbI_2Br$	1.19	0.72	13.91	[15]
P3HT	Free	$CsPbI_2Br$	1.24	0.67	14.35	[16]
P3HT	Free	$CsPbI_2Br$	1.26	0.65	15.50	[17]
P3HT	Free	$CsPbI_2Br$	1.30	0.61	15.69	[18]
P3HT	Free	$CsPbI_2Br$	1.32	0.59	15.90	[19]
P3HT	Free	$CsPbI_2Br$	1.31	0.6	16.30	[20]
P3HT	Free	$CsPbI_2Br$	1.38	0.53	16.93	[21]
P3HT	**Free**	**$CsPbI_2Br$**	**1.43**	**0.48**	**18.39**	**This work**

Table S6. Statistical photovoltaic parameters of control and PP3-treated $CsPbI_3$ PSCs.

Condition	V_{oc} (V)	J_{sc} (mA cm^{-2})	FF	PCE (%)
$CsPbI_3$	1.12±0.03	21.07±0.09	0.78±0.02	18.35±0.59
$CsPbI_3$/PP3	1.19±0.01	21.18±0.08	0.82±0.01	20.77±0.42

Table S7. Summary of photovoltaic parameters for state-of-the-art inorganic $CsPbI_3$ PSCs with dopant-free HTLs.

HTL	Dopant	Perovskite	V_{oc} (V)	V_{oc} loss (V)	PCE (%)	Ref.
CI-TTIN-2F	Free	$CsPbI_3$	1.10	0.60	15.91	[22]
P3HT	Free	$CsPbI_3$	1.09	0.61	17.13	[23]
P3HT	Free	$CsPbI_3$	1.10	0.60	17.92	[24]
P3CT-N	Free	$CsPbI_3$	1.07	0.63	16.67	[25]
P3CT-N	Free	$CsPbI_3$	1.10	0.60	18.21	[26]
P3CT-N	Free	$CsPbI_3$	1.176	0.524	18.93	[27]
P3CT-N	Free	$CsPbI_3$	1.172	0.528	19.01	[28]
P3CT-N	Free	$CsPbI_3$	1.160	0.54	19.25	[29]
P3CT-N	Free	$CsPbI_3$	1.225	0.475	19.27	[30]
P3CT-N	Free	$CsPbI_3$	1.213	0.487	19.84	[31]
P3CT	Free	$CsPbI_3$	1.13	0.58	20.17	[32]
MeO-2PACz	Free	$CsPbI_3$	1.16	0.58	20.17	[33]
PTAA	Free	$CsPbI_3$	1.21	0.49	19.69	[34]
P3HT	**Free**	**$CsPbI_3$**	**1.21**	**0.49**	**21.42**	**This work**

Table S8. Summary of photovoltaic parameters for state-of-the-art inorganic $CsPbI_3$ PSCs with dopant-free P3HT HTLs.

HTL	Dopant	Perovskite	V_{oc} (V)	PCE (%)	Certified PCE (%)	Ref.
P3HT	Free	$FAMAPb(IBr)_3$	1.152	23.3	22.7	[35]
P3HT	Free	$FAMAPb(IBr)_3$	1.09	20.67	/	[36]
P3HT:CuPc	Free	$CsFAMAPb(IBr)_3$	1.24	23.17	21.698 (1 cm^2)	[37]
P3HT:CuPc	Free	$CsFAMAPb(IBr)_3$	1.200	23.38	23.33 (1 cm^2)	[38]
P3HT	Free	$FAMAPb(IBr)_3$	1.15	24.6	/	[39]
P3HT	Free	$MAPbI_3$	1.150	21.1	/	[40]
P3HT	Free	$CsFAMAPb(IBr)_3$	1.15	21.2	/	[41]
P3HT	Free	$CsFAMAPb(IBr)_3$	1.16	22.87	/	[42]
P3HT:NiPc	Free	$FAMAPb(IBr)_3$	1.11	23.11	/	[43]
P3HT	**Free**	**$CsFAPbI_3$**	**1.17**	**25.08**	**24.54**	**This work**

Table S9. Statistical photovoltaic parameters of control and PP3-treated $CsFAPbI_3$ PSCs.

Condition	V_{oc} (V)	J_{sc} (mA cm^{-2})	FF	PCE (%)
$CsFAPbI_3$	1.08±0.01	25.68±0.13	0.75±0.02	21.00±0.40
$CsFAPbI_3$/PP3	1.16±0.01	25.88±0.06	0.80±0.01	24.21±0.36

References

[1] Q. Xiao, J. Tian, Q. Xue, J. Wang, B. Xiong, M. Han, Z. Li, Z. Zhu, H.-L. Yip, Z. a. Li, *Angew. Chem. Int. Ed.* **2019**, *58*, 17724-17730.

[2] K. Jiang, J. Wang, F. Wu, Q. Xue, Q. Yao, J. Zhang, Y. Chen, G. Zhang, Z. Zhu, H. Yan, L. Zhu, H.-L. Yip, *Adv. Mater.* **2020**, *32*, 1908011.

[3] P. Wang, H. Wang, M. Jeong, S. M. Lee, B. Du, Y. Mao, F. Ye, H. Zhang, D. Li, D. Liu, C. Yang, T. Wang, *J. Mater. Chem. C* **2020**, *8*, 8507-8514.
[4] D.-J. Xue, Y. Hou, S.-C. Liu, M. Wei, B. Chen, Z. Huang, Z. Li, B. Sun, A. H. Proppe, Y. Dong, M. I. Saidaminov, S. O. Kelley, J.-S. Hu, E. H. Sargent, *Nat. Commun.* **2020**, *11*, 1514.
[5] X. Li, W. Chen, S. Wang, G. Xu, S. Liu, Y. Li, Y. Li, *Adv. Funct. Mater.* **2021**, 2010696.
[6] P. Wang, H. Wang, Y. Mao, H. Zhang, F. Ye, D. Liu, T. Wang, *Adv. Sci.* **2020**, *7*, 2000421.
[7] J. Wang, X. Wu, Y. Liu, T. Qin, K. Zhang, N. Li, J. Zhao, R. Ye, Z. Fan, Z. Chi, Z. Zhu, *Adv. Energy Mater.* **2021**, *11*, 2100967.
[8] S. Yuan, Y. Xian, Y. Long, A. Cabot, W. Li, J. Fan, *Adv. Funct. Mater.* **2021**, *31*, 2106233.
[9] B. Parida, J. Ryu, S. Yoon, S. Lee, Y. Seo, J. S. Cho, D.-W. Kang, *J. Mater. Chem. A* **2019**, *7*, 18488-18498.
[10] S. Mu, Q. Ye, X. Zhang, S. Huang, J. You, *Front. Optoelectron.* **2020**, *13*, 265-271.
[11] F. Yang, D. Hirotani, G. Kapil, M. A. Kamarudin, C. H. Ng, Y. Zhang, Q. Shen, S. Hayase, *Angew. Chem. Int. Ed.* **2018**, *57*, 12745-12749.
[12] C. F. J. Lau, M. Zhang, X. Deng, J. Zheng, J. Bing, Q. Ma, J. Kim, L. Hu, M. A. Green, S. Huang, A. Ho-Baillie, *ACS Energy Lett.* **2017**, *2*, 2319-2325.
[13] H. Aqoma, I. F. Imran, F. T. A. Wibowo, N. V. Krishna, W. Lee, A. K. Sarker, D. Y. Ryu, S.-Y. Jang, *Adv. Energy Mater.* **2020**, *10*, 2001188.
[14] Z. Wang, A. K. Baranwal, M. A. Kamarudin, Y. Kamata, C. H. Ng, M. Pandey, T. Ma, S. Hayase, *J. Mater. Chem. A* **2019**, *7*, 20390-20397.
[15] Z. Wang, A. K. Baranwal, M. Akmal kamarudin, P. Zhang, G. Kapil, T. Ma, S. Hayase, *Nano Energy* **2019**, *66*, 104180.
[16] J. H. Heo, D. H. Kim, J. K. Park, Y. K. Choi, D. S. Lee, S. H. Im, *ACS Appl. Mater. Interfaces* **2019**, *11*, 43066-43074.
[17] M.-H. Li, S.-C. Liu, F.-Z. Qiu, Z.-Y. Zhang, D.-J. Xue, J.-S. Hu, *Adv. Energy Mater.* **2020**, 2000501.
[18] S. S. Mali, J. V. Patil, J. A. Steele, S. R. Rondiya, N. Y. Dzade, C. K. Hong, *ACS Energy Lett.* **2021**, *6*, 778-788.
[19] Y. Ding, Q. Guo, Y. Geng, Z. Dai, Z. Wang, Z. Chen, Q. Guo, Z. Zheng, Y. Li, E. Zhou, *Nano Today* **2022**, *46*, 101586.
[20] J. Song, H. Xie, E. L. Lim, Y. Li, T. Kong, Y. Zhang, X. Zhou, C. Duan, D. Bi, *Solar RRL* **2022**, *6*, 2100880.
[21] M.-H. Li, J.-Y. Shao, Y. Jiang, F.-Z. Qiu, S. Wang, J. Zhang, G. Han, J. Tang, F. Wang, Z. Wei, Y. Yi, Y.-W. Zhong, J.-S. Hu, *Angew. Chem. Int. Ed.* **2021**, *60*, 16388-16393.
[22] C. Liu, C. Igci, Y. Yang, O. A. Syzgantseva, M. A. Syzgantseva, K. Rakstys, H. Kanda, N. Shibayama, B. Ding, X. Zhang, V. Jankauskas, Y. Ding, S. Dai, P. J. Dyson, M. K. Nazeeruddin, *Angew. Chem. Int. Ed.* **2021**, *60*, 20489-20497.
[23] Z. SunLi, Y. Liu, S. Li, J. Ren, Y. Wu, Q. Sun, Y. Cui, M. Chen, Y. Hao, *ACS Appl. Mater. Interfaces* **2022**, *14*, 7417-7427.
[24] W. Ren, Y. Liu, Y. Wu, Q. Sun, Y. Cui, Y. Hao, *Phys. Chem. Chem. Phys.* **2021**, *23*, 23818-23826.
[25] S. Fu, L. Wan, W. Zhang, X. Li, W. Song, J. Fang, *ACS Energy Lett.* **2020**, *5*, 3314-3321.

[26] Z. Xu, N. Liu, X. Liu, W. Han, W. Xu, J. Zhang, L. Huang, Z. Hu, Y. Zhu, *Chem. Eng. J.* **2023**, *451*, 139047.
[27] S. Fu, W. Zhang, X. Li, J. Guan, W. Song, J. Fang, *ACS Energy Lett.* **2021**, *6*, 3661-3668.
[28] C. Lu, X. Li, X. Guo, S. Fu, W. Zhang, H. Yuan, J. Fang, *Chem. Eng. J.* **2022**, 139495.
[29] S. Fu, X. Li, J. Wan, W. Zhang, W. Song, J. Fang, *Adv. Funct. Mater.* **2022**, *32*, 2111116.
[30] S. Fu, N. Sun, J. Le, W. Zhang, R. Miao, W. Zhang, Y. Kuang, W. Song, J. Fang, *ACS Appl. Mater. Interfaces* **2022**, *14*, 30937-30945.
[31] S. Fu, J. Le, X. Guo, N. Sun, W. Zhang, W. Song, J. Fang, *Adv. Mater.* **2022**, *34*, 2205066.
[32] S. Wang, M.-H. Li, Y. Zhang, Y. Jiang, L. Xu, F. Wang, J.-S. Hu, *Energy Environ. Sci.* **2023**, *16*, 2572-2578.
[33] R. Ji, Z. Zhang, Y. J. Hofstetter, R. Buschbeck, C. Hänisch, F. Paulus, Y. Vaynzof, *Nat. Energy* **2022**, *7*, 1170-1179.
[34] J. H. Heo, F. Zhang, J. K. Park, H. Joon Lee, D. S. Lee, S. J. Heo, J. M. Luther, J. J. Berry, K. Zhu, S. H. Im, *Joule* **2022**, *6*, 1672-1688.
[35] J. J. Yoo, G. Seo, M. R. Chua, T. G. Park, Y. Lu, F. Rotermund, Y.-K. Kim, C. S. Moon, N. J. Jeon, J.-P. Correa-Baena, V. Bulović, S. S. Shin, M. G. Bawendi, J. Seo, *Nature* **2021**, *590*, 587-593.
[36] Y.-W. Jang, S. Lee, K. M. Yeom, K. Jeong, K. Choi, M. Choi, J. H. Noh, *Nat. Energy* **2021**, *6*, 63-71.
[37] J. Peng, D. Walter, Y. Ren, M. Tebyetekerwa, Y. Wu, T. Duong, Q. Lin, J. Li, T. Lu, M. A. Mahmud, O. L. C. Lem, S. Zhao, W. Liu, Y. Liu, H. Shen, L. Li, F. Kremer, H. T. Nguyen, D.-Y. Choi, K. J. Weber, K. R. Catchpole, T. P. White, *Science* **2021**, *371*, 390-395.
[38] J. Peng, F. Kremer, D. Walter, Y. Wu, Y. Ji, J. Xiang, W. Liu, T. Duong, H. Shen, T. Lu, F. Brink, D. Zhong, L. Li, O. Lee Cheong Lem, Y. Liu, K. J. Weber, T. P. White, K. R. Catchpole, *Nature* **2022**, *601*, 573-578.
[39] M. J. Jeong, K. M. Yeom, S. J. Kim, E. H. Jung, J. H. Noh, *Energy Environ. Sci.* **2021**, *14*, 2419-2428.
[40] F. Cheng, R. He, S. Nie, C. Zhang, J. Yin, J. Li, N. Zheng, B. Wu, *J. Am. Chem. Soc.* **2021**, *143*, 5855-5866.
[41] F. Cao, F. Cheng, X. Huang, X. Dai, Z. Tang, S. Nie, J. Yin, J. Li, N. Zheng, B. Wu, *Adv. Funct. Mater.* **2022**, *32*, 2201423.
[42] D. Xu, Z. Gong, Y. Jiang, Y. Feng, Z. Wang, X. Gao, X. Lu, G. Zhou, J.-M. Liu, J. Gao, *Nat. Commun.* **2022**, *13*, 7020.
[43] H. Kim, D. Y. Lee, J. Lim, J. Kim, J. Park, J. Seidel, J. S. Yun, S. I. Seok, *Adv. Energy Mater.* **2023**, *13*, 2301046.